Kinetic-anisotropy-induced ordering-orientation transitions calculated in CoPt alloys under various epitaxial growth conditions

Lin Shi and Jun Ni
Department of Physics and Key Laboratory of Atomic and Molecular Nanoscience (Ministry of Education), Tsinghua University, Beijing 100084, People's Republic of China
(Received 25 March 2007; published 8 January 2008)

We have investigated the epitaxial growth of CoPt alloy under various growth conditions. We find the equilibrium phase changes from the $L1_0$ [100] ordered structure to the $L1_0$ [001] ordered structure with the increase of the underlayer lattice constant parallel to the substrate plane. We show that there are two types of ordering-orientation transitions induced by kinetic anisotropy. When the lattice constant of underlayer is large, the ordered structure of CoPt films changes from the $L1_0$ [001] variant to the $L1_0$ [100] variant with the increase of growth rate. When the lattice constant of underlayer is small, the ordered structure of CoPt films changes from the $L1_0$ [100] variant to the $L1_0$ [001] variant, and then changes to $L1_0$ [100] variant with the increase of growth rate. These ordering-orientation transitions also occur with the decrease of temperature at adequate growth rate. We show that the underlayer with large lattice constant and the Pt buffer layer are suitable for the formation of the $L1_0$ [001] ordered structure.

DOI: 10.1103/PhysRevB.77.035407 PACS number(s): 81.15.Aa, 64.60.Cn, 68.55.−a

I. INTRODUCTION

The epitaxial methods have been extensively used in alloy growth for the purpose of fabricating various ordered structures.[1–7] The epitaxial methods are used to prepare the highly ordered CoPt and FePt alloys films. For the CoPt and FePt alloys, the structure is a face-centered-cubic (fcc) structure with disordered state or is a face-centered-tetragonal (fct) $L1_0$ structure with ordered state. The growth of fct alloy films with the $L1_0$ bulk structure has three equivalent orientation variants: the $L1_0$ [100], [010], and [001] ordered structures as shown in Fig. 1. The magnetic anisotropy and Kerr rotation of CoPt and FePt alloys are sensitive to the chemical ordering, and many experiments have been devoted to growing the highly ordered structure under different conditions.[8–34] The substrate and buffer layer are important in the formation of the ordered structures. For improving the crystal orientation and order parameter, and lowering the ordering temperature, the Pt buffer layer is grown on the substrate MgO or glass before the alloy film growth.[11–18] In some experiments, the Ag underlayers[19,20] or Cr underlayers[21] are added between the Pt buffer layers and MgO substrates. The alloy films can also be grown on the Ag buffer layers[22–26] or the Cr buffer layers.[27] The intensity of CoPt(001) peak increases with the increase of Ag layer thickness.[24] The lattice constants of Pt, Ag, and Cr are all larger than that of CoPt, which can increase the lattice constant of CoPt in the film direction. The Cu buffer layers are used to grow the alloy films.[28,29] The Cu buffer layer, whose lattice constant is smaller than that of CoPt, can decrease the lattice constant and change the magnetic anisotropy from out of plane to in plane with the increase of the Cu buffer layer thickness.[29] The Ag buffer layer is more suitable for forming $L1_0$ [001] ordered structure than the Cu buffer layer.[30] Metal alloys have been also used as the underlayer materials, for example, the CrX (X=Ru,Mo,W,Ti) underlayers[31,32] or the RuAl underlayers[33] are inserted between the Pt buffer layers and substrates. Changing the concentration ratio of alloy is used to adjust the lattice constant of underlayer to affect the structure and properties of the grown thin films.[34]

The growth conditions affect the kinetic process during the epitaxial growth, in particular, the choice of the buffer layer and the underlayer. In our previous work,[35] we show that there is an ordering orientation transition due to the kinetic anisotropy in CoPt alloy. In this work, we show rich ordering features under various growth conditions. We find the equilibrium phase changes from the $L1_0$ [100] ordered structure to the $L1_0$ [001] ordered structure with the increase of the lattice constant parallel to the substrate plane. This leads to two types of variation paths of ordered structures with the increase of growth rate and temperature. When the lattice constant is large, we show that the ordered structure of CoPt films changes from the $L1_0$ [001] variant to the $L1_0$ [100] variant with the increase of growth rate. When the lattice constant is small, the ordered structure of CoPt films changes from the $L1_0$ [100] variant to the $L1_0$ [001] variant, and then changes to the $L1_0$ [100] variant with the increase of growth rate.

The outline of this work is as follows. In Sec. II, we describe the methods. In Sec. III, we show the results and discuss the effects of growth conditions on the formation of the ordered structure of CoPt films. Finally, we give a summary in Sec. IV.

II. METHODS

We consider an fct thin film of CoPt alloy grown in the (001) direction. In fct structure, the lateral lattice constant a

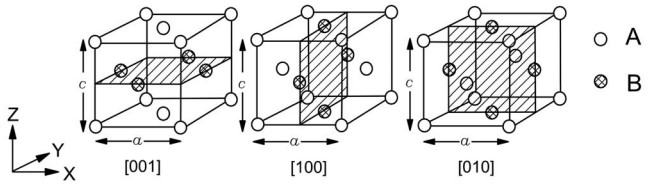

FIG. 1. The [001], [100], and [010] variants of the $L1_0$ ordered structure.

is different from the longitudinal lattice constant c, and the interaction energies in the lateral plane are different from those between the layers. We describe the system by the stochastic lattice gas model with the Hamiltonian

$$\mathcal{H} = H_0 + \sum_s E^{(0)} c_{\mathrm{Co}}^s + \sum_{ij} \sum_{ss'_{\parallel}} E_{ij}^{(1)\parallel} c_i^s c_j^{s'_{\parallel}} + \sum_{ij} \sum_{ss''_{\parallel}} E_{ij}^{(2)\parallel} c_i^s c_j^{s''_{\parallel}} + \sum_{ij} \sum_{ss'_{\perp}} E_{ij}^{(1)\perp} c_i^s c_j^{s'_{\perp}} + \sum_{ij} \sum_{ss''_{\perp}} E_{ij}^{(2)\perp} c_i^s c_j^{s''_{\perp}}, \quad (1)$$

where H_0 is the energy constant, $E^{(0)}$ is the energy per Co atom, $E_{ij}^{(1)\parallel}$ is the nearest-neighbor interaction energy in the lateral plane, $E_{ij}^{(2)\parallel}$ is the next nearest-neighbor interaction energy in the lateral plane, and $E_{ij}^{(1)\perp}$ and $E_{ij}^{(2)\perp}$ are the nearest- and next-nearest-neighbor interaction energies between the layers. The variable $c_i^s=1$ if the site s is occupied by $i(=\mathrm{Co},\mathrm{Pt})$ species and is zero otherwise. The first sum runs over all sites, the second sum runs over all the nearest-neighbor sites in the lateral plane, the third sum runs over all the next-nearest-neighbor sites in the lateral plane, and the last two sums run over all the nearest- and next-nearest-neighbor sites between the layers. The interaction energies $E_{ij}^{(k)}$ affect the equilibrium ordered structures of the system only through the interchange energy $J^{(k)}=\frac{1}{4}(E_{\mathrm{CoCo}}^{(k)}+E_{\mathrm{PtPt}}^{(k)}-2E_{\mathrm{CoPt}}^{(k)})$. When $J^{(k)}>0$, the system tends to form an ordered phase, and when $J^{(k)}<0$, the system becomes phase separation.

In order to calculate the ordering process, we have determined the structural parameters and interaction energies in the kinetic equations by performing the calculations of the total energies of structures using VASP (the Vienna *ab initio* simulation package).[36] The approach is based on an iterative solution of the Kohn-Sham equations of the density-functional theory in a plane-wave basis set with the Vanderbilt ultrasoft pseudopotentials.[37] The exchange correlation functional with the generalized gradient approximation is given by Perdew *et al.*[38] We set the plane-wave cutoff energy to be 500 eV. The tolerance of the energy convergence is 10^{-4} eV. In order to determine the accurate interchange energies, we have employed the same size of supercells for different structures. The calculations are performed on the $(2\times2\times1)$ supercells containing 16 atoms. A mesh of gamma centered grids $5\times5\times9$ is used to sample the Brillouin zone.

For a binary alloy consisting of atoms A and B on a lattice of fixed symmetry, the total energy can be expressed as[39]

$$E(r) = \sum_n v_n(r)\xi_n, \quad (2)$$

where $v_n(r)$ are many-body interaction potentials, the ξ_n are multisite correlation functions defined on an nth order cluster, r is a lattice constant, and the sum is over all cluster types on a fixed lattice. We choose six important interaction potentials, v_n, $n=0-5$, to be determined from the total energy calculations. ξ_0 represents the structure-independent term. ξ_1 is the point correlation function. ξ_2, ξ_3, and ξ_4 correspond to the nearest pairs, triangles, and tetrahedra. ξ_5 corresponds to the next-nearest pairs.

We need to calculate the energies of both fcc and fct ($a\neq c$) structures to determine the energy parameters in Eq. (1). The energies of Co, Pt, $\mathrm{Co_3Pt}(L1_2)$, $\mathrm{CoPt}(L1_0)$, $\mathrm{CoPt}(L1_1)$, and $\mathrm{CoPt_3}(L1_2)$ in fcc structure with different lattice constants are calculated. We use the approach of Kozłowski[40,41] to calculate interaction energies and get

$$J_{fcc}^{(1)}(r) = \frac{1}{6}v_2(r),$$

$$E_{\mathrm{CoPt}}^{(1)fcc}(r) = \frac{1}{6}[v_0(r) - v_2(r)],$$

$$E_{\mathrm{CoCo}}^{(1)fcc}(r) = \frac{1}{6}[v_0(r) + v_1(r) + v_2(r)],$$

$$E_{\mathrm{PtPt}}^{(1)fcc}(r) = \frac{1}{6}[v_0(r) - v_1(r) + v_2(r)]. \quad (3)$$

The next-nearest-neighbor interaction energies are small, and we calculate them by $E_{\mathrm{CoPt}}^{(2)}(r)=-\frac{1}{2}J_{fcc}^{(2)}(r)=-\frac{1}{2}v_5(r)$ and $E_{\mathrm{CoCo}}^{(2)}(r)=E_{\mathrm{PtPt}}^{(2)}(r)=0.0$ eV. The equilibrium structure is only determined by the interchange energy $J_{fcc}^{(i)}$, and $E_{ij}^{(2)}(r)$ has little effects on the kinetics of growth.

For the fct structure, the distances of the nearest pairs in the lateral plane and between the layers are different. We have distinguished the nearest pairs in the lateral plane and the nearest pairs between the layers as different pair energies. We have $v_2^{\parallel}$ and $v_2^{\perp}$, which correspond the nearest pair interaction potential in the lateral plane and the nearest pair interaction potential between the layers, respectively. Under the approach by Kozłowski,[41] we get

$$J^{(1)} = \frac{1}{2}v_2^{\parallel},$$

$$J_{\perp}^{(1)} = \frac{1}{4}v_2^{\perp}. \quad (4)$$

Only the interchange energies can be deduced directly, and we need to approximate other interaction energies for the fct structures by those of the fcc structures with the same lattice constants. Since the next-nearest-neighbor interaction energies are very small, we do not distinguish their direction dependence and determine them by the results in the fcc structures.

During the epitaxial growth process, the system consists of three components, two atomic species (Co and Pt), and vacancy (V). The lattice of (001) planes of an fct alloy is the square lattice. To describe the ordering of the system, we divide the square lattice of each layer into two sublattices (α and β). The configurations of the system are described by the site probabilities in the kinetic mean-field approximation of growth.[42,43] $P_i^s(m,t)$ is the probability occupied by $i(=\mathrm{Co},\mathrm{Pt},\mathrm{V})$ species in $s(=\alpha,\beta)$ sublattices on the mth growth layer at time t. In the calculation, the site probabilities satisfy the following normalization conditions:

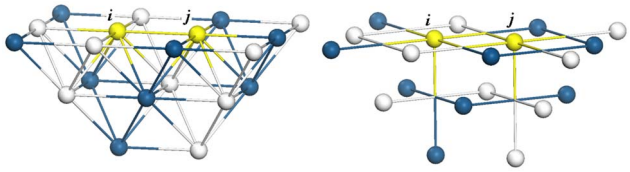

FIG. 2. (Color online) The neighboring sites for the exchange in the plane: blue (dark gray) site is the s sublattice and white (light gray) site is s' sublattice. (a) The nearest-neighbor interactions; (b) the next-nearest-neighbor interactions.

$$\sum_{i(\mathrm{Co,Pt,V})} P_i^{\alpha}(m,t) = 1, \quad \sum_{i(\mathrm{Co,Pt,V})} P_i^{\beta}(m,t) = 1. \tag{5}$$

The concentrations of each layer are related to the site probability P_i^s as follows: $x_i(m)=[P_i^{\alpha}(m)+P_i^{\beta}(m)]/2$. The phase structures are described by the following order parameters in each layer related to the site probability P_i^s. The order parameter in the [100] direction is $\eta_{[100]}(m)=P_{\mathrm{Co}}^{\alpha}(m)-P_{\mathrm{Co}}^{\beta}(m)$. The order parameter in the [001] direction[17] is $\eta_{[001]}(m)=|x_{\mathrm{Co}}(m)-x_{\mathrm{Pt}}(m)|$. The order parameters equal to 1 correspond the complete ordering. When the order parameter of an orientation variant is zero, the system is disordered for this orientation variant. When the order parameter takes fractional value, the ordering in that direction is partial, which means that the corresponding sublattices are not completely occupied by one species of atoms (Co or Pt atoms).

In the kinetics of growth, there are the three contributions from the diffusion, adsorption, and evaporation processes.[42,43] For the diffusion process, we can define the basic exchange probability function $Y_{ij}^{ss'}(m,l)$, which represents the exchange probability between species i on the site s of the mth layer and species j on the site s' of the lth layer per unit time. $Y_{ij}^{ss'}(m,l)$ is proportional to the atomic exchange rate, the site probabilities $P_i^s(m)$ and $P_j^{s'}(l)$, the activation energy factor $\exp(-\beta U_{ij})$, and the bond broken factor $w_{ij}^{ss'}(m,l)$ describing the effect of the neighboring sites for the exchange.[44,45] The growth process satisfies the solid on solid restriction condition, and $Y_{ij}^{ss'}(m,l)$ is proportional to the vacancy probability of the layer above the top layer, $P_V(k)$ $[k=\max(m,l)+1]$. Then, $Y_{ij}^{ss'}(m,l)$ is given by

$$Y_{ij}^{ss'}(m,l) = \nu P_i^s(m) P_j^{s'}(l) \exp(-\beta U_{ij}) w_{ij}^{ss'}(m,l) P_V(k). \tag{6}$$

We consider only the exchange between nearest neighbors, so the relation between m and l is $l-m=0,\pm 1$. The diffusion rate depends on the local atomic configuration.[45] Each atomic exchange is affected by the interaction with the species on the neighboring sites. In the site approximation, the summation over the neighboring configurations can be given by a more computational efficient product of sums.[45] This product factor due to the interaction changes of the exchange species with the neighboring species in the atomic exchange is called the bond broken factor. In our work, we consider not only the neighboring sites in the plane but also the neighboring sites in the substrates. For the exchange in the plane, the neighboring sites are shown in Fig. 2. In Fig. 2(a), the bonds are the nearest-neighbor interactions. In Fig. 2(b), the bonds are the next-nearest-neighbor interactions. The bond broken factor $w_{ij}^{ss'}(m,m)$ for the exchange in the plane is given as follows:

$$\begin{aligned}
w_{ij}^{ss'}(m,m) = {} & \left\{ \sum_{k=\mathrm{CoPtV}} P_k^s(m) \exp\left[-\frac{\beta}{2}(E_{ik}^{(1)\parallel} - E_{jk}^{(1)\parallel}) \right] \exp\left[-\frac{\beta}{2}(E_{jk}^{(2)\parallel} - E_{ik}^{(2)\parallel}) \right] \right\}^2 \left\{ \sum_{k=\mathrm{CoPtV}} P_k^{s'}(m) \exp\left[-\frac{\beta}{2}(E_{jk}^{(1)\parallel} - E_{ik}^{(1)\parallel}) \right] \right. \\
& \left. \times \exp\left[-\frac{\beta}{2}(E_{ik}^{(2)\parallel} - E_{jk}^{(2)\parallel}) \right] \right\}^2 \left\{ \sum_{k=\mathrm{CoPtV}} P_k^s(m) \exp\left[-\frac{\beta}{2}(E_{jk}^{(2)\parallel} - E_{ik}^{(2)\parallel}) \right] \right\}^2 \left\{ \sum_{k=\mathrm{CoPtV}} P_k^{s'}(m) \right. \\
& \left. \times \exp\left[-\frac{\beta}{2}(E_{ik}^{(2)\parallel} - E_{jk}^{(2)\parallel}) \right] \right\}^2 \left\{ \sum_{k=\mathrm{CoPtV}} P_k^{s'}(m) \exp\left[-\frac{\beta}{2}(E_{jk}^{(1)\parallel} - E_{ik}^{(1)\parallel}) \right] \right\} \left\{ \sum_{k=\mathrm{CoPtV}} P_k^s(m) \exp\left[-\frac{\beta}{2}(E_{ik}^{(1)\parallel} - E_{jk}^{(1)\parallel}) \right] \right\} \\
& \times \left\{ \sum_{k=\mathrm{CoPtV}} P_k^s(m-1) \exp\left[-\frac{\beta}{2}(E_{jk}^{(1)\perp} - E_{ik}^{(1)\perp}) \right] \right\} \left\{ \sum_{k=\mathrm{CoPtV}} P_k^{s'}(m-1) \exp\left[-\frac{\beta}{2}(E_{jk}^{(1)\perp} - E_{ik}^{(1)\perp}) \right] \right\} \left\{ \sum_{k=\mathrm{CoPtV}} P_k^s(m-1) \right. \\
& \left. \times \exp\left[-\frac{\beta}{2}(E_{ik}^{(1)\perp} - E_{jk}^{(1)\perp}) \right] \right\} \left\{ \sum_{k=\mathrm{CoPtV}} P_k^{s'}(m-1) \exp\left[-\frac{\beta}{2}(E_{ik}^{(1)\perp} - E_{jk}^{(1)\perp}) \right] \right\} \left\{ \sum_{k=\mathrm{CoPtV}} P_k^s(m-2) \right. \\
& \left. \times \exp\left[-\frac{\beta}{2}(E_{jk}^{(2)\perp} - E_{ik}^{(2)\perp}) \right] \right\} \left\{ \sum_{k=\mathrm{CoPtV}} P_k^{s'}(m-2) \exp\left[-\frac{\beta}{2}(E_{ik}^{(2)\perp} - E_{jk}^{(2)\perp}) \right] \right\}.
\end{aligned} \tag{7}$$

For the exchange between the layers, the neighboring sites are shown in Fig. 3. The bond broken factor $w_{ij}^{ss'}(m,m-1)$ for the exchange between the layers is given as follows:

$$w_{ij}^{ss'}(m,m-1)=\left\{\sum_{k=\mathrm{CoPtV}}P_k^s(m)\exp\left[-\frac{\beta}{2}(E_{jk}^{(2)\parallel}-E_{ik}^{(2)\parallel})\right]\exp\left[-\frac{\beta}{2}(E_{ik}^{(1)\perp}-E_{jk}^{(1)\perp})\right]\right\}\left\{\sum_{k=\mathrm{CoPtV}}P_k^s(m)\right.$$
$$\times\exp\left[-\frac{\beta}{2}(E_{jk}^{(2)\parallel}-E_{ik}^{(2)\parallel})\right]\Big\}^3\left\{\sum_{k=\mathrm{CoPtV}}P_k^{s'}(m)\exp\left[-\frac{\beta}{2}(E_{jk}^{(1)\parallel}-E_{ik}^{(1)\parallel})\right]\right\}^2\left\{\sum_{k=\mathrm{CoPtV}}P_k^{s'}(m)\exp\left[-\frac{\beta}{2}(E_{jk}^{(1)\parallel}-E_{ik}^{(1)\parallel})\right]\right.$$
$$\times\exp\left[-\frac{\beta}{2}(E_{ik}^{(1)\perp}-E_{jk}^{(1)\perp})\right]\Big\}^2\left\{\sum_{k=\mathrm{CoPtV}}P_k^{s}(m-1)\exp\left[-\frac{\beta}{2}(E_{ik}^{(1)\parallel}-E_{jk}^{(1)\parallel})\right]\right\}^2\left\{\sum_{k=\mathrm{CoPtV}}P_k^{s}(m-1)\right.$$
$$\times\exp\left[-\frac{\beta}{2}(E_{ik}^{(1)\parallel}-E_{jk}^{(1)\parallel})\right]\exp\left[-\frac{\beta}{2}(E_{jk}^{(1)\perp}-E_{ik}^{(1)\perp})\right]\Big\}^2\left\{\sum_{k=\mathrm{CoPtV}}P_k^{s'}(m-1)\exp\left[-\frac{\beta}{2}(E_{ik}^{(2)\parallel}-E_{jk}^{(2)\parallel})\right]\right.$$
$$\times\exp\left[-\frac{\beta}{2}(E_{jk}^{(1)\perp}-E_{ik}^{(1)\perp})\right]\Big\}\left\{\sum_{k=\mathrm{CoPtV}}P_k^{s'}(m-1)\exp\left[-\frac{\beta}{2}(E_{ik}^{(2)\parallel}-E_{jk}^{(2)\parallel})\right]\right\}^3\left\{\sum_{k=\mathrm{CoPtV}}P_k^{s}(m-2)\right.$$
$$\times\exp\left[-\frac{\beta}{2}(E_{ik}^{(1)\perp}-E_{jk}^{(1)\perp})\right]\exp\left[-\frac{\beta}{2}(E_{jk}^{(2)\perp}-E_{ik}^{(2)\perp})\right]\Big\}\left\{\sum_{k=\mathrm{CoPtV}}P_k^{s}(m-2)\exp\left[-\frac{\beta}{2}(E_{ik}^{(1)\perp}-E_{jk}^{(1)\perp})\right]\right\}$$
$$\times\left\{\sum_{k=\mathrm{CoPtV}}P_k^{s'}(m-2)\exp\left[-\frac{\beta}{2}(E_{ik}^{(1)\perp}-E_{jk}^{(1)\perp})\right]\right\}^2\left\{\sum_{k=\mathrm{CoPtV}}P_k^{s'}(m-3)\exp\left[-\frac{\beta}{2}(E_{ik}^{(1)\parallel}-E_{jk}^{(1)\perp})\right]\right\}. \quad (8)$$

The broken factor $w_{ij}^{ss'}(m,m+1)$ is similar with $w_{ij}^{ss'}(m,m-1)$.

For the adsorption process, we define $X_i^s(m)$ as the adsorption probability of the species i on the sublattice s of the mth layer per unit time. $X_i^s(m)$ is proportional to the adsorption rate ω_i, the vacancy probability $P_V^s(m)$, and the probability for underlayer occupied by atoms $[\Pi_{\alpha,\beta}(P_{\mathrm{Co}}^s(m-1)+P_{\mathrm{Pt}}^s(m-1))]^2$. Then, $X_i^s(m)$ is given by

$$X_i^s(m)=\omega_i P_V^s(m)[\Pi_{\alpha,\beta}(P_{\mathrm{Co}}^s(m-1)+P_{\mathrm{Pt}}^s(m-1))]^2. \quad (9)$$

For the evaporation process, we define $Z_i^s(m)$ as the evaporation probability of the species i on the s sublattice of the mth layer per unit time. An atom can only evaporate when the sites over it are occupied by vacancies. $Z_i^s(m)$ is proportional to the evaporation rate ω_i', the site probability $P_i^s(m)$ of the evaporation atom, the chemical potential factor $\exp(-\mu_i/k_BT)$ (μ_i is the chemical potential of the i species), the bond broken factor V_i^s for evaporation, and the probability for the sites over it occupied by vacancies. Then, $Z_i^s(m)$ is given by

$$Z_i^s(m)=-\omega_i'\exp(-\mu_i/k_BT)V_i^sP_i^s(m)[P_V^\alpha(m+1)P_V^\beta(m+1)]^2. \quad (10)$$

The bond broken factor $V_i^s(m)$ describes the effect of the neighboring sites for the evaporation. We consider only nearest-neighbor and next-nearest-neighbor interactions, and the bond broken factor $V_i^s(m)$ is given by

$$V_i^s(m)=\left\{\sum_{k=\mathrm{CoPtV}}P_k^{s'}(m)\exp[\beta E_{ik}^{(1)\parallel}]\right\}^4\left\{\sum_{k=\mathrm{CoPtV}}P_k^{s}(m)\exp[\beta E_{ik}^{(2)\parallel}]\right\}^4\left\{\sum_{k=\mathrm{CoPtV}}P_k^{s}(m-1)\exp[\beta E_{ik}^{(1)\perp}]\right\}^2$$
$$\times\left\{\sum_{k=\mathrm{CoPtV}}P_k^{s'}(m-1)\exp[\beta E_{ik}^{(1)\perp}]\right\}^2\left\{\sum_{k=\mathrm{CoPtV}}P_k^{s}(m-2)\exp[\beta E_{ik}^{(2)\perp}]\right\}. \quad (11)$$

The adsorption rate is related to the evaporation rate by the detailed balance condition.[42]

From the above analysis, we can get the following differential equations describing the kinetics of growth:

$$\frac{dP_i^s(m)}{dt}=\sum_j\sum_{s'}(Y_{ji}^{ss'}-Y_{ij}^{ss'})+X_i^s(m)+Z_i^s(m), \quad (12)$$

where the first sum runs over all nearest sites of the i species on the site s. Since the vacancy probabilities satisfy the normalization conditions, we consider the site probabilities of the two atomic species (Co and Pt) on the two sublattices in all film layers. There are $2\times2\times8$ differential equations, solved numerically by the Runge-Kutta method. Since the diffusion, adsorption, and evaporation processes are affected by the neighboring layers, the site probabilities are correlated and the equations are solved simultaneously. Initially, the growth layer is empty and the buffer layer is Pt layer. We

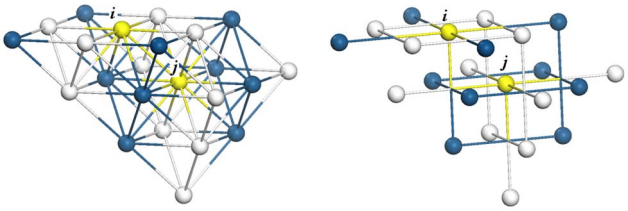

FIG. 3. (Color online) The neighboring sites for the exchange between the layers: blue (dark gray) site is the s sublattice and white (light gray) site is s' sublattice. (a) The nearest-neighbor interactions; (b) the next-nearest-neighbor interactions.

give the evolution of the occupied probabilities based on the differential equations.

In the kinetic process, we take the activation energy of atomic diffusion as follows: The activation energy for the surface diffusion of Pt atoms is taken as 0.47 eV, which is the activation energy for Pt diffusion on the Pt(001) surface,[46] and the activation energy for the surface diffusion of Co atoms is taken as 0.58 eV, which is the activation energy for Co diffusion on the Co(001) surface.[47] For the bulk diffusion in CoPt(001) multilayers, the activation energy is 1.1 eV.[48] Since the atomic jumping frequency is approximately 10^{14} s^{-1}, we take the prefactor $\nu_D=\tau_D^{-1}=10^{14}$ s^{-1}. The surface diffusion is much faster than the bulk diffusion for the CoPt epitaxial growth.

III. RESULTS

In epitaxial growth, CoPt thin films with a certain lattice mismatch with the substrate are grown. The lattice constant of the thin film can be changed in the substrate direction due to the mismatch.[49] The initial growth of the thin films on the substrate is pseudomorphic growth with uniaxial distortion of the films. There are limitations on the thickness of pseudomorphic growth. As long as the film thickness is below the critical thickness, a matched film can be grown on a substrate. In the epitaxial growth of CoPt alloy, the thickness of the underlayer is about 30 nm and the thickness of the Pt buffer layer is about 4 nm.[31,32] Since the thickness of the Pt buffer layer is small and its lattice constant is decided by that of the underlayer, the lattice constant of initial CoPt growth layer is decided by the lattice constant of the underlayer. We can change the lattice constant of the underlayer to adjust that of CoPt growth layer and Pt buffer layer.

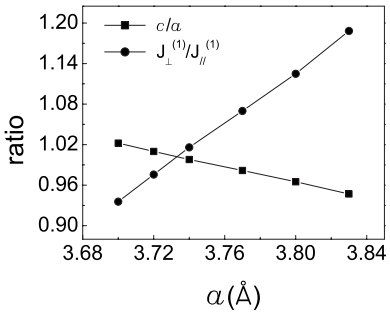

FIG. 4. The ratios c/a and $J_{\perp}^{(1)}/J_{\parallel}^{(1)}$ as functions of the lattice constant a.

A. Interaction energies and the equilibrium phases

We have calculated the structural parameters, energy parameters and binding energies as shown in Table I. Figure 4 shows the ratios c/a and $J_{\perp}^{(1)}/J_{\parallel}^{(1)}$ as a function of the lattice constant a. The ratio c/a decreases from 1.022 to 0.947 with the increase of the lattice constant a from 3.70 to 3.83 Å. In our previous work,[35] we have considered the case of fcc lattice with $a=3.77$ Å. In this work, we find that the fcc case corresponds to the one with lattice constant $a\simeq 3.74$ Å. The kinetic features for fct lattice with $a>3.74$ Å are also similar

TABLE I. The structural parameters, energy parameters and binding energy E of CoPt alloys with different lattice constants.

	1	2	3	4	5	6
a (Å)	3.83	3.80	3.77	3.74	3.72	3.70
c (Å)	3.63	3.67	3.70	3.73	3.76	3.78
$E_{\mathrm{CoPt}}^{(1)\parallel}$ (eV)	−0.916	−0.905	−0.891	−0.875	−0.864	−0.851
$E_{\mathrm{CoCo}}^{(1)\parallel}$ (eV)	−0.732	−0.732	−0.729	−0.725	−0.723	−0.718
$E_{\mathrm{PtPt}}^{(1)\parallel}$ (eV)	−0.914	−0.881	−0.844	−0.804	−0.775	−0.744
$E_{\mathrm{CoPt}}^{(1)\perp}$ (eV)	−0.637	−0.718	−0.796	−0.872	−0.928	−0.987
$E_{\mathrm{CoCo}}^{(1)\perp}$ (eV)	−0.558	−0.617	−0.671	−0.726	−0.764	−0.803
$E_{\mathrm{PtPt}}^{(1)\perp}$ (eV)	−0.495	−0.599	−0.696	−0.794	−0.868	−0.946
$E_{\mathrm{CoPt}}^{(2)\parallel}$ (eV)	0.014	0.014	0.015	0.015	0.015	0.015
$E_{\mathrm{CoPt}}^{(2)\perp}$ (eV)	0.016	0.016	0.015	0.015	0.015	0.015
$J_{\parallel}^{(1)}$ (eV)	0.0463	0.0493	0.0523	0.0555	0.0578	0.0600
$J_{\perp}^{(1)}$ (eV)	0.0550	0.0553	0.0558	0.0563	0.0563	0.0560
E[001] (eV/atom)	−4.194	−4.485	−4.757	−5.017	−5.210	−5.408
E[100] (eV/atom)	−4.159	−4.462	−4.741	−5.014	−5.216	−5.424

to the results in our previous work.[35] Since the evaporation probability and the difference between the interaction energies for Co and for Pt are small, the concentrations of each species are mainly decided by the adsorption rates. The adsorption rates for Co and for Pt are the same. The calculated results shows that the fluctuations of concentrations are smaller than 0.01, so it is considered as equiatomic growth. The interaction energies $E_{ij}^{(k)}$ affect the equilibrium phase transition of the system only through the interchange energies. We have also calculated the interchange energies of different orientations at different lattice constants as shown in Table I. We have calculated the binding energy E by the interaction energy parameters as shown in Table I. It can be seen that when $a>c$, $J_{\perp}^{(1)}/J_{\parallel}^{(1)}>1$ and the binding energy $E[001]$ for the $L1_0$ [001] ordered structure is lower than $E[100]$ for the $L1_0$ [100] ordered structure. The $L1_0$ [001] ordered structure is the equilibrium phase. When $a<c$, $J_{\perp}^{(1)}/J_{\parallel}^{(1)}<1$ and $E[001]$ is higher than $E[100]$. The $L1_0$ [100] ordered structure is the equilibrium phase. With the increase of a, the ratio $J_{\perp}^{(1)}/J_{\parallel}^{(1)}$ increases from 0.936 to 1.188, and the equilibrium phase changes from the $L1_0$ [100] ordered structure to the $L1_0$ [001] ordered structure. This change leads to various features in the kinetic process.

The equilibrium phase corresponds to the phase formed in the kinetic process at small growth rate. In addition to the lattice constant of the substrate, the other factors which affect the kinetic process are the growth temperature, the growth rate, and the buffer layer. The higher the growth temperature is, the faster the atoms diffuse and the easier the system reaches equilibrium phase. The growth rate also affects the diffusion. When the growth rate is large, the surface is covered quickly and the time for diffusion is short, and then the system reaches disorder phase or metastable phase. When the growth rate is small, the time for diffusion is long which is suitable for forming ordered structure. We choose the Pt buffer layer which is generally used in experiments. Since Pt and Co tend to be nearest neighbors, the Pt buffer layer tends to result in the growth of Co atom in the first layer which favors the formation of the $L1_0$ [001] ordered structure. The whole kinetic process is determined by all these factors, and the resulted structures are varied under different growth conditions.

When the various transitions between the $L1_0$ [001] ordered structure and the $L1_0$ [100] ordered structure occur, the lattice parameters and the interaction energies will change. For the case of complete ordering, since the parallel lattice parameter a is decided by the underlayer, we fix only a to calculate the binding energies for various orientations by the first principles method. Table II shows the binding energy difference $\Delta E=E[001]-E[100]$. The lattice constant c of the $L1_0$ [001] ordered structure is smaller than that of the $L1_0$ [100] ordered structure. The binding energy difference increases with the decrease of the lattice constant a. We have also calculated the binding energy differences from the energy parameters. The binding energy difference calculated from the energy parameters also increases with the decrease of the lattice constant a. They show the same variation tendency, and the energy differences are small. Thus, the energy parameters can describe the energy change under the ordering-orientation transitions approximately.

TABLE II. The binding energy difference between two ordering orientations calculated by the first principles method and by energy parameters.

a (Å)	ΔE (eV) (calculated by VASP)	ΔE (eV) (by energy parameters)
3.83	−0.025	−0.035
3.80	−0.013	−0.023
3.77	−0.005	−0.016
3.74	0.007	−0.003
3.72	0.013	0.006
3.70	0.023	0.016

B. Order parameters versus κ

Then, we study the effects of the growth rate on the growth kinetic process. We define the ratio $\kappa=\omega/\nu_D$ between the deposition rate ω and atomic jumping frequency ν_D and use κ as a parameter. Since the equilibrium phases are different for different lattice constants, we have calculated the order parameters as a function of κ for different lattice constants as shown in Fig. 5. $\bar{\eta}$ is the average value of the four intermediate layers to avoid the effect of the substrate and surface. When $a=3.83$ Å and $c=3.63$ Å as shown in Fig. 5(a), the [001] direction is the dominant ordering direction in the whole kinetic process. $\overline{\eta_{[100]}}$ has a peak, but its value is always lower than $\overline{\eta_{[001]}}$. In this case, $J_{\perp}^{(1)}/J_{\parallel}^{(1)}>1$ and $J_{\perp}^{(1)}$ is the dominant energy. The Pt buffer layer also leads to the $L1_0$ [001] ordered structure. The surface diffusion process for forming the [100] variant becomes less effective. Thus, with the decrease of growth rate, the $L1_0$ [001] ordered structure forms and the average order parameter $\overline{\eta_{[001]}}$ is higher than $\overline{\eta_{[100]}}$. In the case of $a>c$, the equilibrium phase is the $L1_0$ [001] ordered structure. When a decreases and c increases, the kinetic process of surface diffusion for the $L1_0$ [100] ordered structure becomes more effective. The structure first changes from the $L1_0$ [001] variant to the $L1_0$ [100] variant, and then the structure changes to the disordered state with the increase of the growth rate as shown in Figs. 5(b)–5(d), which is similar to our previous results.[35] The peak value and the width of $\overline{\eta_{[100]}}$ increase with the decrease of the lattice constant a. When $J_{\perp}^{(1)}$ is almost equal to $J_{\parallel}^{(1)}$, the surface diffusion process for the formation of the $L1_0$ [100] variant becomes important. The $L1_0$ [100] ordered structure forms at a larger growth rate although the equilibrium phase is the $L1_0$ [001] ordered structure. When $a<c$, the equilibrium phase is the $L1_0$ [100] ordered structure. The ordering-orientation first changes from the [100] direction to the [001] direction, then changes to the [100] direction, and finally the structure changes to the disordered state with the increase of growth rate as shown in Figs. 5(e) and 5(f). In these cases, $J_{\perp}^{(1)}/J_{\parallel}^{(1)}<1$, which leads to the stable $L1_0$ [100] ordered structure. The pure diffusion process will not lead to the

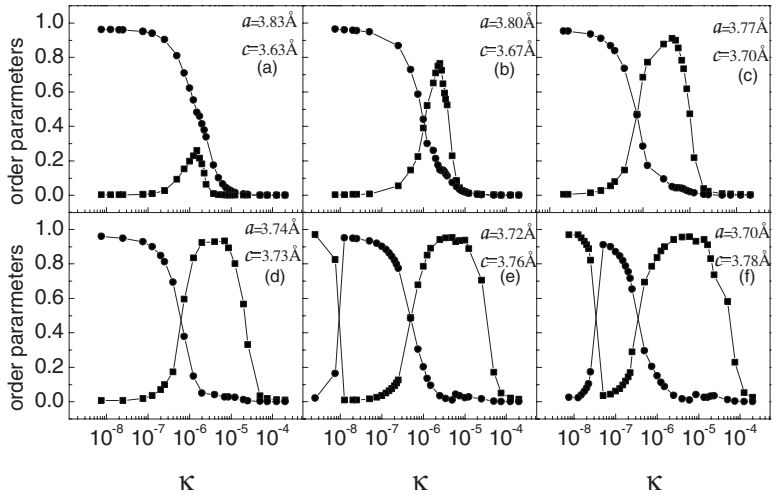

FIG. 5. The order parameters with the change of κ for different lattice constants with $T=630$ K, where circles represent $\overline{\eta_{[001]}}$ and squares represent $\overline{\eta_{[100]}}$.

formation of the $L1_0$ [001] ordered structure. However, the Pt buffer layer prefers the formation of the $L1_0$ [001] ordered structure and has an opposite effect with the interchange energies. The ordering process is rather complex in this case. There is a peak in the curve of the order parameter for the $L1_0$ [001] variant and a corresponding valley in the curve of the order parameter for the $L1_0$ [100] variant as shown in Figs. 5(e) and 5(f). With the decrease of a, the width of $\overline{\eta_{[001]}}$ peak decreases. In these cases, the Pt buffer layer becomes less effective and $J_{\parallel}^{(1)}$ becomes more effective due to $J_{\perp}^{(1)}/J_{\parallel}^{(1)}$ decreases with the decrease of a.

Now, we analyze the whole kinetic feature of the ordering-orientation transition shown in Fig. 5(f). When the growth rate is very small ($\kappa=7.5\times10^{-9}$), as shown in Figs. 6(a) and 6(b), there are small peaks in the curves of the order parameters for the first layer, which indicates that the atoms tend to form the $L1_0$ [001] ordered structure initially due to the effect of Pt buffer layer. However, atoms have enough time to diffuse, and the equilibrium phase $L1_0$ [100] ordered structure forms finally. When the growth rate increases ($\kappa=5.0\times10^{-8}$), as shown in Figs. 6(c) and 6(d), the atoms do not have enough time to form the equilibrium phase but can diffuse between the different layers. Under the affection of Pt buffer layer, the system forms the $L1_0$ [001] ordered structure and the peak of $\overline{\eta_{[001]}}$ occurs. When the growth rate increases further ($\kappa=6.0\times10^{-6}$), as shown in Figs. 6(e) and 6(f), the atoms have only time to diffuse on the surface. Then, the $L1_0$ [100] ordered structure forms and the peak of $\overline{\eta_{[100]}}$ occurs. In Fig. 5(f), there is a small valley on the peak of $\overline{\eta_{[100]}}$ (the large peak can be considered as consisting of two peaks). The formation mechanism of the small valley is as follows: When the growth rate continues to increase ($\kappa=8.75\times10^{-6}$) after the peak, as shown in Figs. 6(g) and 6(h), the atoms do not have enough time to diffuse in the first layer and the order parameter of the first layer decreases and those of the following layers also decrease, which leads to a decrease of $\overline{\eta_{[100]}}$. When the growth rate increases further ($\kappa=1.35\times10^{-5}$), as shown in Figs. 6(i) and 6(j), atoms have little time to diffuse in the first layer and cannot form ordered layer. However, the disordered layer leads to the high ordered second layer by the mechanism of the oscillatory ordered phase,[43] which leads to the increase of the order parameter in the [100] direction and the formation of the small valley on the peak of $\overline{\eta_{[100]}}$. When the growth rate is very quick ($\kappa=2.0\times10^{-4}$), atoms do not have time to diffuse, and only the disordered phase forms. Under the competition among the effects of all growth parameters, the structure first changes from the $L1_0$ [100] ordered structure to the $L1_0$ [001] ordered structure, then changes back to the $L1_0$ [100] ordered structure, and finally the structure becomes a disordered one with the increase of growth rate.

For comparison, we have also calculated the order parameters as a function of κ for different lattice constants using the Monte Carlo method[50] with the same growth mechanism and energy parameters as those used in the mean-field approach. The simulations are carried out on square 32×32 lattices with eight growing layers. The periodic boundary condition in the x-y plane is used. The square lattices are divided into two sublattices to describe the ordering of the system. The sublattice average occupations are used to calculate the order parameters. Twenty repeated growth procedures are used for the average. As shown in Fig. 7, the curves of the order parameters are consistent with those calculated by the mean-field approach. When $a\geqslant3.80$ Å, the [001] direction is the dominant ordering direction as shown in Figs. 7(a) and 7(b). In the case of $a>c$, when a decreases and c increases, the kinetic process of surface diffusion for the $L1_0$ [100] ordered structure becomes more effective. The structure first changes from the $L1_0$ [001] variant to the $L1_0$ [100] variant, and then the structure changes to the disordered state with the increase of the growth rate as shown in Figs. 7(c) and 7(d). When $a<c$, the $L1_0$ [100] ordered structure becomes the equilibrium phase. When $a=3.72$ Å and $c=3.76$ Å, the ordering-orientation first changes from the [100] direction to the [001] direction, then changes to the [100] direction, and finally the structure changes to the

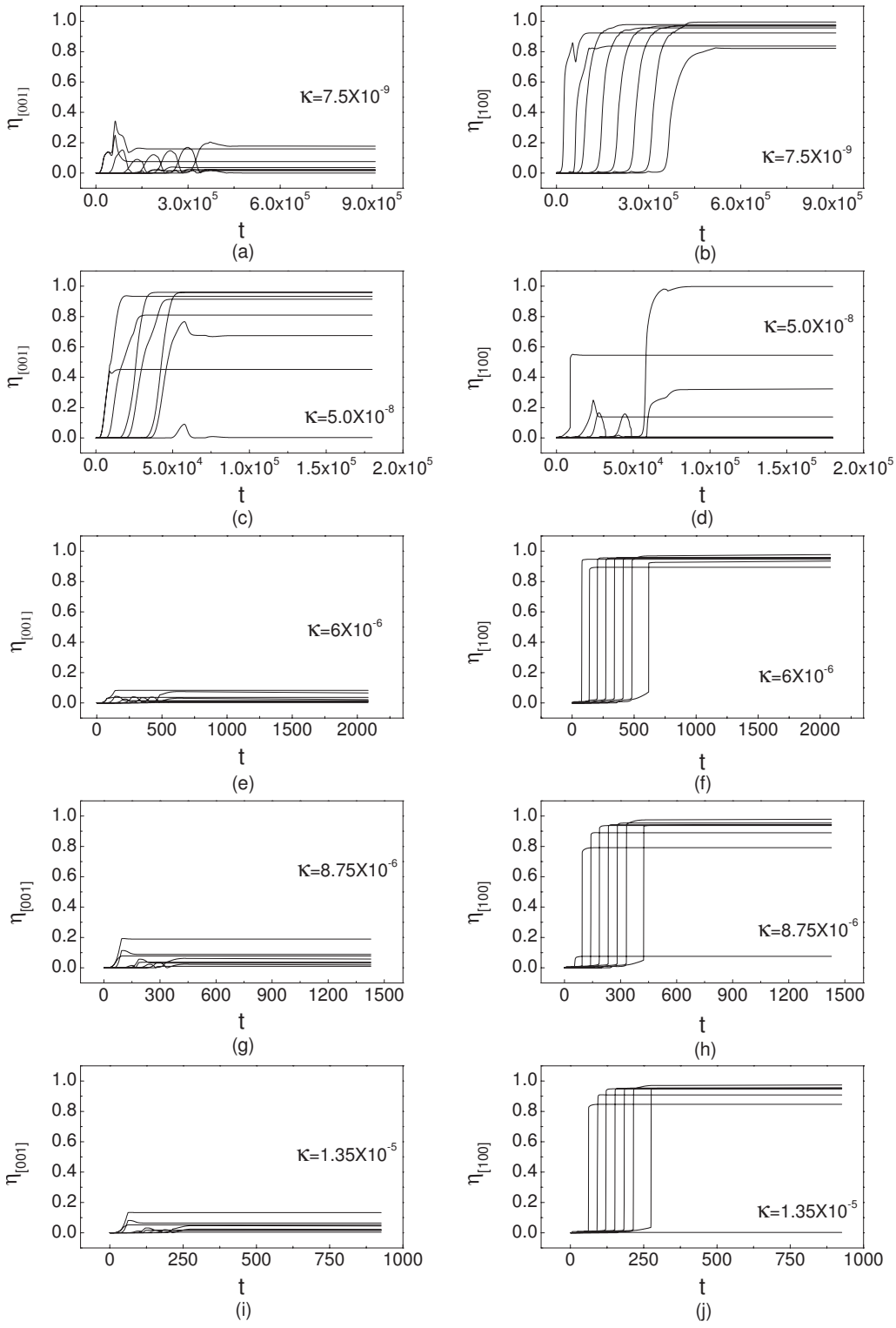

FIG. 6. The evolution of $\eta_{[001]}$ and $\eta_{[100]}$ at different κ with $T=630$ K.

disordered state with the increase of growth rate as shown in Fig. 7(e). When $a=3.70$ Å and $c=3.78$ Å, the [100] direction is the dominant ordering direction in the whole kinetic process as shown in Fig. 7(f). The Monte Carlo method gives slower ordering kinetics than the mean-field approach, which is in agreement with the results of Ref. 51 showing that the evolution time in the pair approximation for the long range order to reach the equilibrium value is longer than that in the site approximation. As the lattice constant a decreases from 3.72 to 3.70 Å, the peak for order parameter in the [001] direction becomes narrower in the results of the mean-field approach, while the peak for order parameter in the [001] direction almost disappeared in the case of $a=3.70\text{Å}$ in the results of the Monte Carlo approach.

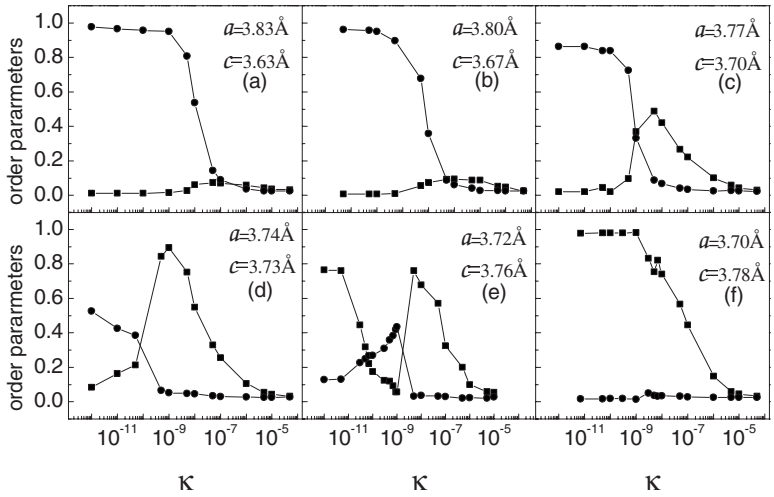

FIG. 7. The order parameters with the change of κ for different lattice constants with $T=630$ K calculated by the Monte Carlo method, where circles represent $\eta_{[001]}$ and squares represent $\eta_{[100]}$.

C. Order parameters versus temperature

The growth temperature is another important growth condition. Now, we study the variation of the order parameters with the growth temperature under different lattice constants. When $a>c$, the variation of the order parameters is shown in Fig. 8, which is similar to the results of our previous work.[35] The atomic diffusion rate increases with the increase of temperature. $\eta_{[001]}$ increases with the increase of the growth temperature, and $\eta_{[100]}$ has a temperature peak when $\kappa < 2.0\times10^{-5}$. The peak value and the width of $\eta_{[100]}$ decrease with the increase of κ. The structure first changes from the $L1_0$ [001] variant to the $L1_0$ [100] variant, and then the structure becomes disordered with the decrease of growth temperature.

When $a<c$, the evolution of the order parameters is shown in Fig. 9, which is different from that in Fig. 8. When the growth rate is very small ($\kappa=2.5\times10^{-7}$) as shown in Fig. 9(a), the system has enough time to diffuse and forms the $L1_0$ [001] ordered structure at the moderate growth temperature due to the effect of the Pt buffer layer. The structure changes from the frozen disordered state to the $L1_0$ [100] ordered structure, then changes to the $L1_0$ [001] ordered structure, and finally the structure becomes the $L1_0$ [100] ordered structure with the increase of growth temperature. When κ decreases to $\kappa=2.5\times10^{-6}$, there is a peak in the curve of $\eta_{[001]}$ and a valley in the curve of $\eta_{[100]}$ as shown in Fig. 9(b). At high temperature and low temperature, both states are the $L1_0$ [100] ordered structures. At the moderate growth temperature, the system tends to form the $L1_0$ [100] ordered structure but only partial ordering is formed due to the large growth rate. When $\kappa=2.5\times10^{-5}$, $\eta_{[001]}$ increases with the increase of the growth temperature, and $\eta_{[100]}$ first increases with the increase of temperature and then decreases

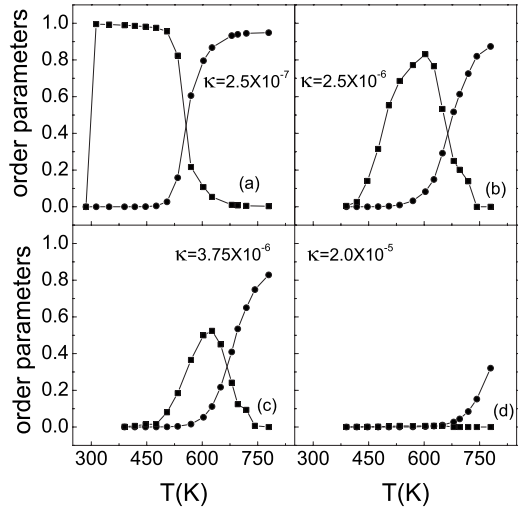

FIG. 8. The order parameters as a function of T at $a=3.80$ Å and $c=3.67$ Å, where circles represent $\eta_{[001]}$ and squares represent $\eta_{[100]}$.

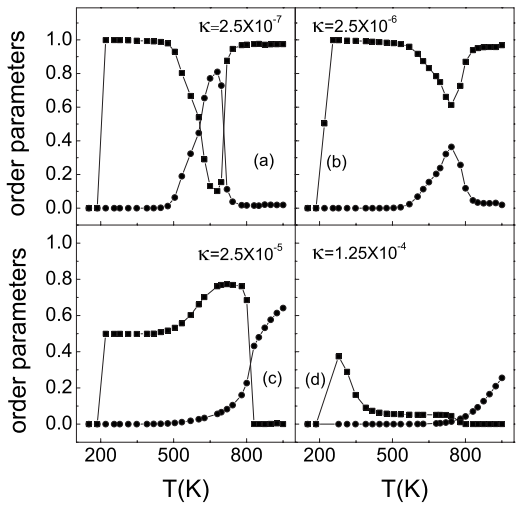

FIG. 9. The order parameters as a function of T at $a=3.70$ Å and $c=3.78$ Å, where circles represent $\eta_{[001]}$ and squares represent $\eta_{[100]}$.

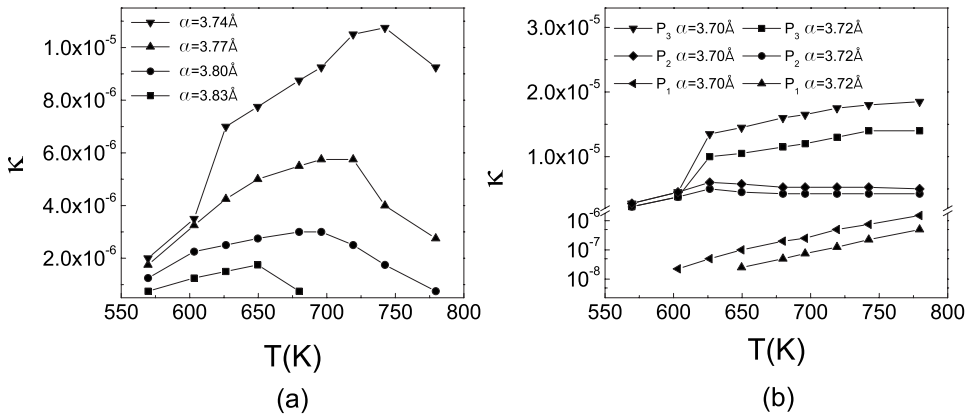

FIG. 10. The κ values of the order parameter peak positions as a function of temperature for different lattice constants: (a) $a \geqslant 3.74$ Å and $J_{\perp}^{(1)}/J_{\parallel}^{(1)} > 1$; (b) $a < 3.74$ Å and $J_{\perp}^{(1)}/J_{\parallel}^{(1)} < 1$.

above $T=700$ K. $\overline{\eta_{[100]}}$ becomes zero at about $T=830$ K as shown in Fig. 9(c). At $T=600-700$ K, the surface diffusion dominates the diffusion process and the $L1_0$ [100] ordered structure forms. When the temperature increases, the diffusion rate increases and the atoms can diffuse between different layers; thus, the $L1_0$ [001] ordered structure forms due to the large growth rate. When $T \approx 400$ K, $\overline{\eta_{[100]}}$ has a plateau and its value is about 0.5, and the structure is the oscillatory ordered phase.[43] When $\kappa = 1.25 \times 10^{-4}$, $\overline{\eta_{[001]}}$ increases with the increase of growth temperature and $\overline{\eta_{[100]}}$ has a small peak at low temperature as shown in Fig. 9(d).

D. Peak positions of average order parameters

We have shown that the kinetic anisotropy leads to a peak of the average order parameter $\bar{\eta}$ with the change of growth rate and temperature, which results in the ordering-orientation transitions. Now, we discuss how the peak positions of the average order parameters change with the growth condition. The κ values of the peak positions as a function of growth temperature are shown in Fig. 10. It can be seen that the κ values increase with the decrease of the lattice constant a at the same growth temperature. Since $J_{\perp}^{(1)}/J_{\parallel}^{(1)}$ decreases with the decrease of a, the corresponding growth rate κ for the formation of the $L1_0$ [100] variant increases.

When $J_{\perp}^{(1)}/J_{\parallel}^{(1)} > 1$, there is only one $\overline{\eta_{[100]}}$ peak and the κ value of the peak position as a function of growth temperature is shown in Fig. 10(a). In the case of $a=3.83$ Å, the peak of $\overline{\eta_{[100]}}$ disappears when the growth temperature is higher than 680 K, which indicates that the ordering in the [100] direction cannot appear when $T > 680$ K for $a=3.83$ Å. In the case of $a=3.80$ Å, the disappearing temperature of the peak is about 780 K. With the decrease of a, the temperature range for the occurrence of the peak increases. When $J_{\perp}^{(1)}/J_{\parallel}^{(1)} < 1$, there are three $\bar{\eta}$ peaks as shown in Fig. 5(d), and their κ values change with the increase of growth temperature as shown in Fig. 10(b). The P_1, P_2, and P_3 correspond to the $\overline{\eta_{[001]}}$ peak position, the first $\overline{\eta_{[100]}}$ peak position, and the second $\overline{\eta_{[100]}}$ peak position with the increase of κ, respectively. The κ value of the $\overline{\eta_{[001]}}$ peak position increases with the increase of growth temperature. When $T < 600$ K, there is only one $\overline{\eta_{[100]}}$ peak. With the increase of growth temperature, the oscillatory ordered phase occurs and the $\overline{\eta_{[100]}}$ peak is divided into two peaks (P_2 and P_3). P_2 decreases slightly with the increase of growth temperature. P_3 increases with the increase of growth temperature. If there was no oscillatory ordered phase, the $\overline{\eta_{[100]}}$ peak would be between P_2 and P_3 and the corresponding κ value would increase with the increase of growth temperature.

Based on the above analysis of the kinetic process in the epitaxial growth, we find that the underlayer in the substrate with larger lattice constant is suitable for the formation of the $L1_0$ [001] ordered structure, and the underlayer with smaller lattice constant is suitable for the formation of the $L1_0$ [100] ordered structure. The Pt buffer layer also plays an important role in the kinetics of ordering during the epitaxial growth, which helps in the formation of the $L1_0$ [001] ordered structure. In order to form the $L1_0$ [001] ordered structure with the important application easily, it is better to choose the Pt buffer layer and the larger lattice constant underlayer. For the underlayer with moderate lattice constant, we can adjust the growth rate and the growth temperature to obtain different ordering-orientation transitions.

IV. SUMMARY

We have investigated the effects of the various growth conditions on the kinetic process during epitaxial growth. In the CoPt film epitaxial growth on the Pt buffer layers and underlayers with different lattice constants, we show that the ratio of $J_{\perp}^{(1)}/J_{\parallel}^{(1)}$ increases with the increase of the lattice constant a. When $a > 3.74$ Å, $J_{\perp}^{(1)} > J_{\parallel}^{(1)}$. The equilibrium phase is the $L1_0$ [001] ordered structure. At moderate growth temperature such as $T=630$ K, the structure first changes from the $L1_0$ [001] ordered variant to the $L1_0$ [100] ordered variant, and then the structure becomes disordered with the increase of growth rate. The ordering-orientation transition also occurs with the change of temperature. $\overline{\eta_{[001]}}$ increases with the increase of the growth temperature and $\overline{\eta_{[100]}}$ has a temperature peak at adequate growth rate. The peak value

and the width of $\overline{\eta_{[100]}}$ decrease with the increase of growth rate. The peak of $\eta_{[100]}$ becomes smaller at large growth rate. On the other hand, when $a<3.74$ Å, $J_{\perp}^{(1)}<J_{\parallel}^{(1)}$. The equilibrium phase is the $L1_0$ [100] ordered structure. When $a=3.72$ Å and $c=3.76$ Å, the ordering orientation first changes from the [100] direction to the [001] direction, then changes to the [100] direction, and finally the structure becomes disordered with the increase of growth rate at moderate growth temperature. The grown structure depends on the growth temperature. At small growth rate, the structure changes from the frozen disordered state to the $L1_0$ [100] ordered structure, then changes to the $L1_0$ [001] ordered structure, and finally the structure becomes the $L1_0$ [100] ordered structure with the increase of the growth temperature. At moderate growth rate, $\eta_{[001]}$ has a temperature peak and $\overline{\eta_{[100]}}$ has a temperature valley. At large growth rate, $\overline{\eta_{[001]}}$ increases with the increase of growth temperature and $\overline{\eta_{[100]}}$ has a temperature peak. We have determined the variation of the peak positions of the order parameters with the change of growth condition. The κ value of the $\overline{\eta_{[100]}}$ peak position increases with the decrease of the lattice constant a. In order to form the $L1_0$ [001] ordered structure easily, the substrate should have the Pt buffer layer and the underlayer with large lattice constant. For the occurrence of the different ordering-orientation transitions, it is better to choose the underlayer with moderate lattice constant.

ACKNOWLEDGMENTS

This research was supported by the National Natural Science Foundation of China under Grant No. 10674076 and the National Basic Research Program of China (2006CB605105).

[1] A. Ourmazd and J. C. Bean, Phys. Rev. Lett. **55**, 765 (1985).
[2] T. S. Kuan, T. F. Kuech, W. I. Wang, and E. L. Wilkie, Phys. Rev. Lett. **54**, 201 (1985).
[3] G. L. Zhou, M. H. Yang, and C. P. Flynn, Phys. Rev. Lett. **77**, 4580 (1996).
[4] J. H. He, C. A. Carosella, G. K. Hubler, S. B. Qadri, and J. A. Sprague, Phys. Rev. Lett. **96**, 056105 (2006).
[5] I. Daruka and J. Tersoff, Phys. Rev. Lett. **95**, 076102 (2005).
[6] J. L. Stevens and R. Q. Hwang, Phys. Rev. Lett. **74**, 2078 (1995).
[7] G. Abadias, I. Schuster, A. Marty, and B. Gilles, Phys. Rev. B **61**, 6495 (2000).
[8] S. Okamoto, N. Kikuchi, O. Kitakami, T. Miyazaki, Y. Shimada, and K. Fukamichi, Phys. Rev. B **66**, 024413 (2002).
[9] T. Shima, T. Seki, K. Takanashi, Y. K. Takahashi, and K. Hono, J. Magn. Magn. Mater. **272-276**, e557 (2004).
[10] R. A. Ristau, K. Barmak, L. H. Lewis, K. R. Coffey, and J. K. Howard, J. Appl. Phys. **86**, 4527 (1999).
[11] A. Cebollada, D. Weller, J. Sticht, G. R. Harp, R. F. C. Farrow, R. F. Marks, R. Savoy, and J. C. Scott, Phys. Rev. B **50**, 3419 (1994).
[12] R. F. C. Farrow, D. Weller, R. F. Marks, M. F. Toney, S. Hom, G. R. Harp, and A. Cebollada, Appl. Phys. Lett. **69**, 1166 (1996).
[13] R. F. C. Farrow, D. Weller, R. F. Marks, M. F. Toney, A. Cebollada, and G. R. Harp, J. Appl. Phys. **79**, 5967 (1996).
[14] R. F. C. Farrow, D. Weller, R. F. Marks, M. F. Toney, D. J. Smith, and M. R. McCartney, J. Appl. Phys. **84**, 934 (1998).
[15] W. Grange, C. Ulhaq-Bouillet, M. Maret, and J. Thibault, Acta Mater. **49**, 1439 (2001).
[16] M. Abes, O. Ersen, D. Muller, M. Acosta, C. Ulhaq-Bouillet, A. Dinia, and V. Pierron-Bohnes, Mater. Sci. Eng., C **23**, 229 (2003).
[17] O. Ersen, V. Parasote, V. Pierron-Bohnes, M. C. Cadeville, and C. Ulhaq-Bouillet, J. Appl. Phys. **93**, 2987 (2003).
[18] K. Barmak, J. Kim, L. H. Lewis, K. R. Coffey, M. F. Toney, A. J. Kellock, and J.-U. Thiele, J. Appl. Phys. **98**, 033904 (2005).
[19] S. Iwata, S. Yamashita, and S. Tsunashima, IEEE Trans. Magn. **33**, 3670 (1997).
[20] Y. N. Hsu, S. Jeong, D. E. Laughlin, and D. N. Lambeth, J. Magn. Magn. Mater. **260**, 282 (2003).
[21] A. C. Sun, P. C. Kuo, J. H. Hsu, H. L. Huang, and J. M. Sun, J. Appl. Phys. **98**, 076109 (2005).
[22] Y. N. Hsu, S. Jeong, D. E. Laughlin, and D. N. Lambeth, J. Appl. Phys. **89**, 7068 (2001).
[23] Y. Xu, Z. G. Sun, Y. Qiang, and D. J. Sellmyer, J. Magn. Magn. Mater. **266**, 164 (2003).
[24] X. H. Xu, Z. G. Yang, and H. S. Wu, J. Magn. Magn. Mater. **295**, 106 (2005).
[25] X. H. Xu, H. S. Wu, F. Wang, and X. L. Li, Thin Solid Films **472**, 222 (2005).
[26] Z. L. Zhao, J. S. Chen, J. Ding, J. B. Yi, B. H. Liu, and J. P. Wang, Appl. Phys. Lett. **88**, 052503 (2006).
[27] Y. F. Ding, J. S. Chen, E. Liu, and L. Li, J. Magn. Magn. Mater. **303**, e238 (2006).
[28] C. J. Sun, G. M. Chow, and J. P. Wang, Appl. Phys. Lett. **82**, 1902 (2003).
[29] Y. F. Ding, J. S. Chen, and E. Liu, Surf. Coat. Technol. **198**, 262 (2005).
[30] X. H. Xu, H. S. Wu, F. Wang, and X. L. Li, Appl. Surf. Sci. **233**, 1 (2004).
[31] J. S. Chen, B. C. Lim, Y. F. Ding, and G. M. Chow, J. Magn. Magn. Mater. **303**, 309 (2006).
[32] B. C. Lim, J. S. Chen, and J. P. Wang, Surf. Coat. Technol. **198**, 296 (2005).
[33] W. K. Shen, J. H. Judy, and J. P. Wang, J. Appl. Phys. **97**, 10H301 (2005).
[34] Y. F. Xu, J. S. Chen, and J. P. Wang, Appl. Phys. Lett. **80**, 3325 (2002).
[35] L. Shi and J. Ni, Phys. Rev. Lett. **97**, 126105 (2006).
[36] G. Kresse and J. Hafner, Phys. Rev. B **47**, R558 (1993); **49**, 14251 (1994); G. Kresse and J. Furthmüller, *ibid.* **54**, 11169 (1996).
[37] D. Vanderbilt, Phys. Rev. B **41**, R7892 (1990).
[38] J. P. Perdew, J. A. Chevary, S. H. Vosko, K. A. Jackson, M. R. Pederson, D. J. Singh, and C. Fiolhais, Phys. Rev. B **46**, 6671 (1992).
[39] J. W. D. Connolly and A. R. Williams, Phys. Rev. B **27**, 5169

(1983).
[40] M. Kozłowski, R. Kozubski, V. Pierron-Bohnes, and W. Pfeiler, Comput. Mater. Sci. **33**, 287 (2005).
[41] M. Kozłowski, M.S. thesis, Jagellonian University, 2004.
[42] Y. Saito and H. Müller-Krumbhaar, J. Chem. Phys. **70**, 1078 (1979).
[43] L. Shi and J. Ni, Phys. Rev. B **69**, 155428 (2004).
[44] H. T. Shi and J. Ni, Phys. Rev. B **65**, 115422 (2002).
[45] L. Q. Chen and J. A. Simmons, Acta Metall. Mater. **42**, 2943 (1994).
[46] G. L. Kellogg and P. J. Feibelman, Phys. Rev. Lett. **64**, 3143 (1990).
[47] R. A. Miron and K. A. Fichthorn, Phys. Rev. B **72**, 035415 (2005).
[48] P. C. Mclntyre, D. T. Wu, and M. Nastasi, J. Appl. Phys. **81**, 637 (1997).
[49] J. R. Arthur, Surf. Sci. **500**, 189 (2002).
[50] D. P. Landau and K. Binder, *A Guide to Monte Carlo Simulations in Statistical Physics* (Cambridge University Press, Cambridge, 2000).
[51] L. Q. Chen, Phys. Rev. B **58**, 5266 (1998).